Published in final edited form as:
Circ Res. 2005 June 10; 96(11): 1169–1177. doi:10.1161/01.RES.0000169271.33675.05.

Functional Properties of Mouse Connexin30.2 Expressed in the Conduction System of the Heart

Maria M. Kreuzberg,
Institut für Genetik, Abteilung Molekulargenetik, Universität Bonn, Germany

Goran Söhl,
Institut für Genetik, Abteilung Molekulargenetik, Universität Bonn, Germany

Jung-Sun Kim,
Department of Pathology, Asan Medical Center, University of Ulsan, Seoul, Korea

Vytas K. Verselis,
Department of Neuroscience, Albert Einstein College of Medicine, Bronx, NY

Klaus Willecke, and
Institut für Genetik, Abteilung Molekulargenetik, Universität Bonn, Germany

Feliksas F. Bukauskas
Department of Neuroscience, Albert Einstein College of Medicine, Bronx, NY

Abstract

Gap junction channels composed of connexin (Cx) 40, Cx43, and Cx45 proteins are known to be necessary for impulse propagation through the heart. Here, we report mouse connexin30.2 (mCx30.2) to be a new cardiac connexin that is expressed mainly in the conduction system of the heart. Antibodies raised to the cytoplasmic loop or the C-terminal regions of mCx30.2 recognized this protein in mouse heart as well as in HeLa cells transfected with wild-type mCx30.2 or mCx30.2 fused with enhanced green fluorescent protein (mCx30.2-EGFP). Immunofluorescence analyses of adult hearts yielded positive signals within the sinoatrial node, atrioventricular node, and A-V bundle of the cardiac conduction system. Dye transfer studies demonstrated that mCx30.2 and mCx30.2-EGFP channels discriminate poorly on the basis of charge, but do not allow permeation of tracers >400 Da. Both mCx30.2 and mCx30.2-EGFP gap junctional channels exhibited weak sensitivity to transjunctional voltage (V_j) and a single channel conductance of ≈9 pS, which is the lowest among all members of the connexin family measured in HeLa cell transfectants. HeLa mCx30.2-EGFP transfectants when paired with cells expressing Cx40, Cx43, or Cx45 formed functional heterotypic gap junction channels that exhibited low unitary conductances (15 to 18 pS), rectifying open channel I-V relations and asymmetric V_j dependence. The electrical properties of homo- and hetero-typic junctions involving mCx30.2 may contribute to slow propagation velocity in nodal tissues and directional asymmetry of excitation spread in the AV nodal region.

Keywords

connexin; gap junctions; mCx30.2; sinoatrial node; atrioventricular node

Correspondence to Feliksas F. Bukauskas, Department of Neuroscience, Albert Einstein College of Medicine, 1300 Morris Park Ave, Bronx, NY 10461. fbukausk@aecom.yu.edu.

Gap junction (GJ) channels composed of connexin (Cx) molecules mediate direct intercellular diffusion of ions and small metabolites. Twenty connexin genes have been identified in the mouse genome.[1] Depending on the expression pattern, connexins can form homotypic, heterotypic, or heteromeric channels with highly divergent conductance, permeability and gating properties.[2] Cx40, Cx43, and Cx45 have been identified as the major connexins expressed in the heart.[3,1,4] Cx43 is predominantly found in the atrial and ventricular working myocytes and, to a lesser extent, in peripheral Purkinje fibers, whereas Cx40 and Cx45 are expressed in the conduction system.[5] Cx40 is preferentially found in the atrial myocardium, the A-V bundle and its branches,[6] whereas Cx45 is mainly expressed in the sinoatrial (SA) and atrioventricular (AV) nodes, as well as the A-V bundle and its branches.[3,7,8] Targeted deletion of Cx40 and Cx43[9,10,6,11] revealed the contribution of each of these connexins to heart development and function. Replacement of Cx43 by Cx40 or Cx40 by Cx45 showed that the function of certain cardiac connexins can be compensated by other connexins.[12,13,14]

Mouse connexin30.2 (mCx30.2) and its human orthologue, Cx31.9, have been reported to be expressed in vascular smooth muscle cells, brain, and testis.[15,16] Furthermore, immunopositive signals for mCx30.2 were found in intercalated discs of the heart as well as in interstitial cells and cells of the seminiferous tubules of the testis.[16] Functional analyses of Cx31.9 gap junctions yielded a low unitary conductance (12 to 15 pS) and weak sensitivity to transjunctional voltage (V_j).[15,17] However, functional properties of mCx30.2 GJ channels have not yet been described. Here we report that mCx30.2 is highly expressed in the cardiac conduction system and that mCx30.2 can form functional homotypic as well as heterotypic junctions with all the major cardiac connexins.

Materials and Methods

Expanded Materials and Methods are in the online data supplement at http://circres.ahajournals.org

Functional Cloning, Transfection, RT-PCR Analysis, and mCx30.2 Antibodies

The coding region of mCx30.2 was PCR-amplified, PCR-fragments were cloned into pIRESpuro2 or pIRESpuro2-EGFP vectors that were transfected into HeLa cells. Two peptides derived from the cytoplasmic loop and the C-terminal region of mCx30.2 were used to produce polyclonal mCx30.2 antibodies. Heart cryosections of adult mice and HeLa transfectants were exposed to mCx30.2, Cx40 or Cx43 antibodies.

Electrophysiology and Fluorescence Imaging

Xenopus oocytes were injected with mCx30.2 RNA to study junctional conductance (g_j) by using a dual 2-electrode voltage clamp method. The dual whole-cell voltage clamp method combined with imaging, were used for electrophysiological and dye transfer studies.

Results

Expression of mCx30.2 Transcripts

After screening the HUSAR-derived *mus musculus* EST database (DDJB/GenBank/EMBL, Heidelberg), we identified a sequence tag (Acc. BF580638) with 91.2% similarity to the coding region of mCx30.2 (Acc. AJ414561). This sequence comprised only ≈160 bp of the complete coding sequence encompassing 837 bp, but contained an additional 34 bp upstream of the *Kozak* consensus motif. Most of this presumptive 5′-untranslated region (5′-UTR) could readily be localized ≈700 bp further upstream of the mCx30.2 open reading frame within the genomic sequence (Acc. AL591067). Both the 3′ part of this putatively

spliced 5′-UTR as well as the 5′ part, shortly upstream of the coding region, contained canonical splice donor and acceptor motifs, respectively.[18] We analyzed expression of this splice isoform in heart and brain. Different primers spanning the intron were used to amplify mCx30.2 cDNA by RT-PCR (Figure 1A). Three out of 6 primers yielded amplicons of ≈740 bp, 770 bp, and 825 bp in size (Figure 1B). Data obtained suggested that the 5′ untranslated sequence comprised at least 120 bp in both tissues. Furthermore, no putative splice acceptor site was identified within 240 bp further upstream. Thus, at least 1 spliced mRNA isoform is transcribed from the mCx30.2 gene containing one untranslated exon1 and the complete coding region on exon2 in tissues such as heart and brain.

To investigate the expression pattern of mCx30.2, we performed intron-spanning RT-PCR analyses in different mouse tissues. The expected fragment of 740 bp was found in heart, brain, kidney, lung, testis, and very faintly in liver (Figure 1C).

HeLa Cell Lines Stably Expressing mCx30.2 and mCx30.2-EGFP

To analyze functional properties of mCx30.2 GJs, HeLa cells were stably transfected with DNA coding for mCx30.2 or mCx30.2-EGFP. Expression of mCx30.2 and mCx30.2-EGFP mRNAs was verified after Northern blot hybridization (see Figure 2A). Immunoblots of different HeLaCx30.2 lysates revealed only one fragment of 28 kDa, which was absent in HeLa wild-type cells, whereas in HeLaCx30.2-EGFP cells the signal of the fusion protein was detected (Figure 2B).

Immunofluorescence of HeLaCx30.2 cells revealed a punctate staining pattern characteristic of gap junction plaques. Figure 2C (I-III) shows that in HeLaCx30.2-EGFP cells junctional plaques revealed by immunostaining (I) or by EGFP fluorescence (II) colocalize (III). HeLa cells expressing Cx40 (IV), Cx43 (V), and Cx45 (VI) when incubated with mCx30.2 antibodies did not show any punctate immunofluorescence and exclude cross-reactivity.

Expression of mCx30.2 Protein

Immunostaining of heart cryosections demonstrated that mCx30.2 is expressed in the cardiac conduction system, but not in working cardiomyocytes of atria or ventricles. Punctate mCx30.2 immunofluorescence was detected in areas of the SA node (Figure 3A and 3B), AV node (Figure 3A through 3F) and A-V bundle (Figure 3A through 3J). Left column (a,e,i) shows bright field images stained for acetylcholine esterase (AChE) that facilitate identifying SA node, AV node, and A-V bundle; squares indicate approximate regions from which immunofluorescence images were acquired. Immunofluorescence analysis in consecutive sections revealed that mCx30.2 and Cx40 were not coexpressed within the SA node and showed a rarely overlapping expression pattern within the AV node and A-V bundle. Cx43 (d,h,l) was not present in cardiac conduction system, but was predominant in the ventricular and atrial working myocardium. Because Cx45 antibodies show substantial cross-reactivity with other connexins, we used $Cx45^{+/LacZ}$ mice[19] to analyze coexpression of mCx30.2 and Cx45. Figure 3B shows abundant immunostaining of mCx30.2 in the SA node (b) and the AV node (d), where LacZ signals (blue) are well expressed. Furthermore, we found coexpression of mCx30.2 and Cx45 at the junction of the superior vena cava and the right atrium and in the posterior nodal extension of the AV node (see Figure I-S in online supplement).

Electrical Cell-Cell Coupling and Gating of Homotypic mCx30.2 Junctions

The ability of mCx30.2 to induce electrical coupling was examined in *Xenopus* oocytes and in HeLa cells expressing mCx30.2 or mCx30.2-EGFP. Pairs of *Xenopus* oocytes injected with mCx30.2 mRNA, displayed high levels of coupling (g_j = 2.8±0.87 μS). Normalized initial and steady state G_j-V_j relations are plotted in Figure 4A. Initial G_j (open circles) did

not change significantly with V_js of either polarity. Steady-state G_j (filled circles) was insensitive to V_j up to ±60 mV and declined only modestly with larger V_js. Representative record of transjunctional currents (I_j) measured at V_j steps of both polarities illustrate the slow time course of the decline in I_j (Figure 4B).

Similar to oocytes, coupling in HeLaCx30.2 and HeLa HeLaCx30.2-EGFP cell pairs showed weak voltage dependence (Figure 4C). Steady-state G_j values obtained from HeLa cells expressing mCx30.2 (open circles) or mCx30.2-EGFP (solid circles) were indistinguishable. At modest V_js of either polarity, G_j showed a tendency to increase. G_j decreased at V_js >80 mV.

Heptanol (2 mmol/L), when applied to cell pairs expressing mCx30.2 or mCx30.2-EGFP, produced full uncoupling and relatively fast recovery on washout (Figure 4D). Application of 100% CO_2 also yielded rapid and full uncoupling between cells expressing mCx30.2 or mCx30.2-EGFP, but slow recovery (≈5 minutes) during washout (data not shown).

Conductance and Permeability of mCx30.2 Channels

We examined single channel conductance in HeLa cell pairs expressing mCx30.2 or mCx30.2-EGFP. Experiments were performed in weakly and well-coupled cell pairs with and without application of CO_2, respectively. Figure 4E shows V_j and I_j records during 2 V_j steps and a ramp. A plot of g_j over time indicates 4 equal conductance levels (horizontal lines) ≈9 pS in magnitude, which we ascribe to single channels.

To assess permeability, we measured dye transfer and g_j in HeLaCx30.2-EGFP cell pairs exhibiting at least 1 junctional plaque. Fluorescent dyes examined included Lucifer Yellow (443 Da, net charge, z, equals −2), Alexa Fluor-350 (326 Da, z = −1), ethidium bromide (EtBr; 314 Da, z1), 4′,6-Diamidino-2-phenylindole (DAPI) (279 Da, z2), and propidium iodide (PrI; 415 Da, z2). Typically, a dye-filled patch pipette was used to load 1 cell of a pair with dye by establishing a whole-cell recording. After allowing ≈10 minutes for dye transfer, a whole-cell recording was established in the second cell to measure g_j. In summary, mCx30.2-EGFP junctions demonstrated permeability to Alexa Fluor-350, EtBr, and DAPI (Figure 5A through 5C), but not to PrI and Lucifer yellow (not shown). At least 5 cell pairs were examined for each dye.

Intercellular transfer of Neurobiotin (287 Da, z1), was examined in monolayers of HeLa-WT, HeLaCx43, HeLaCx30.2, and HeLaCx30.2-EGFP cells. The cells were fixed 30 minutes after Neurobiotin microinjection into a single cell within each monolayer (asterisks in Figure 5D). Neurobiotin readily spread to first and second order neighbors in cells expressing Cx43, mCx30.2, and mCx30.2-EGFP, but not in HeLa-WT cells.

Properties of Heterotypic Junctions Formed of mCx30.2 and Other Cardiac Connexins

mCx30.2/Cx40 Heterotypic Junctions—In cocultures of HeLaCx30.2-EGFP and HeLaCx40 cells, we selected cell pairs in which only one cell exhibited EGFP fluorescence and at least 1 junctional plaque was visible in the junctional membrane. Fluorescence intensities of such plaques were approximately half of that of mCx30.2-EGFP homotypic junctions, consistent with fluorescence contributed from only one side of the junction. Formation of mCx30.2-EGFP/Cx40 junctional plaques in these cell pairs was abundant, suggesting that mCx30.2 and Cx40 hemichannels readily dock to form intercellular channels (see Figure II-S(A) in online data supplement).

We found that mCx30.2-EGFP/Cx40 junctions were functional and exhibited an asymmetric steady-state G_j-V_j relation with higher V_j-sensitivity at voltages relatively negative on the mCx30.2 side (Figure 6A). Open circles show steady-state (normalized) G_j evaluated at the

ends of the 20 s voltage steps. The solid line represents G_j measured in response to the 2 slow V_j ramps that changed from 0 to −115 and to +115 mV over periods of 120 s. Representative recordings shown in Figure 6B demonstrate asymmetric V_j-gating in response to voltage steps of +85 and −85 mV applied to the HeLaCx40 cell. I_j and g_j records during repeated V_j ramps of ±20 mV in amplitude demonstrate fast recovery after the end of the positive voltage step (see dashed arrows). Recovery of g_j after the negative step demonstrates 2 components, a fast one (see solid arrows) and a slow one shown by the dashed regression line. During each voltage ramp, g_j was not constant, suggesting that mCx30.2/Cx40 heterotypic channels rectify, ie, the open channel I-V relationship is not linear.

Figure 6C shows a representative I_j record at the single channel level in response to voltage steps (±85 mV) and ramps (± 105 mV) applied to the HeLaCx40 cell of a Cx40/mCx30.2-EGFP cell pair. The open channel current, I_j, rectifies, decreasing significantly when the Cx40 side is made relatively more negative. On average, the conductance of the open state (γ) decreased from ≈27 to ≈12 pS when V_j changed from +100 to −100 mV; γ=≈18 pS at V_j=0 mV. V_j-induced gating events occurred more often when the Cx40 side was relatively positive and gating transitions were mainly to a substate (see dashed arrows), with full closures occurring occasionally. Gating transitions for V_js relatively negative on the Cx40 side were seldom observed, but mainly transited to the fully closed state and appeared to be slow (see asterisk). Therefore, the decrease in G_j at positive V_js in Figure 6A is mainly defined by rectification properties and the slow gating mechanism of mCx30.2 or Cx40, whereas at negative V_js mainly by the fast V_j-sensitive gating mechanism of mCx30.2 and Cx40.

mCx30.2/Cx43 Heterotypic Junctions—In cocultures of HeLaCx30.2-EGFP and HeLaCx43-CFP cells, we selected cell pairs with junctional plaques exhibiting EGFP and CFP fluorescence (see Figure II-S(B) in online data supplement). The steady-state G_j-V_j relation of this heterotypic junction is strongly asymmetric and exhibits an increase in G_j when the cell expressing mCx30.2 is made more positive (Figure 7A). The I_j record shown in Figure 7B demonstrates this asymmetry in V_j-gating with long-duration V_j steps of ±90 and ±100 mV applied to the HeLaCx30.2-EGFP cell. On termination of the positive V_j steps, I_j in response to repeated Vj ramps (±20 mV) gradually decreased to the level before application of the step. Single channel currents, observed on recovery from uncoupling with CO_2, show a nearly linear open channel I-V curve with γ=≈18 pS (Figure 7C). Cx43-EGFP hemichannels have been shown to close only at V_js relatively negative on their side.[2] The reduction in G_j at V_js relatively negative on the mCx30.2 side must represent closure of mCx30.2 hemichannels. The increased apparent V_j sensitivity of mCx30.2 hemichannels compared with that inferred from mCx30.2 homotypic junctions (Figure 4) can be explained by the small conductance of the mCx30.2 hemichannel relative to the Cx43-EGFP hemichannel.[2] In the heterotypic channel, a larger fraction of the applied V_j would drop across the mCx30.2 hemichannel giving the appearance of increased V_j sensitivity.

mCx30.2/Cx45 Heterotypic Junctions—Junctional plaques were also observed between HeLaCx30.2-EGFP cells and N2A cells expressing Cx45-EGFP. Morphological differences between HeLa and N2A cells allowed identification of heterotypic cell pairs (Figure II-S(C) in online supplement; N2A cells are smaller and more round than HeLa cells), whereas EGFP fluorescence allowed assessment of expression levels. mCx30.2/Cx45 junctions are characterized by a markedly asymmetric G_j-V_j relation (Figure 8A). The solid line shows the fit of the data points shown as filled circles with the Boltzmann equation. Steep and sensitive gating occurs at V_js relatively negative on the Cx45 side. Both, this gating polarity and fitting parameters (G_{max}=1.3±0.1, G_{min}=0.17±0.03, A=0.13±0.02, and V_0=6.7±0.02; see Methods in online data supplements) are characteristic for Cx45 V_j-

gating.[20] Representative recordings are shown for voltage steps of ±55 mV (B) and ± 100 mV (C) applied to the Cx45-expressing cell. For V_js negative on the Cx45-EGFP side, I_j decreased substantially and rapidly, whereas for positive V_j steps I_j increased. On termination of the positive V_j step, the increase in I_j slowly returned to the value preceding the steps (see insert). These data are consistent with Cx45 hemichannels being responsible for closure of the mCx30.2/Cx45 junctions observed at V_js relatively positive on the mCx30.2 side.

Single channel recordings show higher open probability at V_js positive on Cx45-EGFP side (Figure 8D). As previously indicated, closure at V_js positive on mCx30.2 side represent closure of Cx45 hemichannels. The single open channel I-V curve is nearly linear; γ=≈17 pS.

Discussion

mCx30.2 Gene Structure and Protein Expression Pattern

Nielsen et al[15] found that the human Cx31.9 gene is comprised of only 1 exon harboring the 5′-UTR, the coding region and the 3′-UTR, although a strong putative splice acceptor site was detected at position −5. We found that the mCx30.2 gene consists of at least 1 untranslated exon1 as well as exon2 containing the uninterrupted coding region of mCx30.2 and the 3′-UTR, as previously described for most other connexin genes.[21] Because a splice donor site at the 3′border of mCx30.2 corresponds to that found in Cx31.9 and exon1 is also located ≈730 bp upstream of the Cx31.9 coding region [Acc. AC080112], it is likely that the splicing pattern is conserved in both orthologous genes.

We detected mCx30.2 protein expression in the cardiac conduction system with particularly high levels in the SA and the AV nodes (Figure 3). mCx30.2 signals were relatively intense within the SA node, which was immunonegative for Cx40 and Cx43. In the AV node, both mCx30.2 and Cx40 are expressed but Cx43 is not. Several reports indicate that Cx40 is preferentially expressed in the fast-conducting His bundle, the ensuing branches and Purkinje terminal fibers.[8,6] Our immunostaining data show that mCx30.2 is predominantly expressed in slow-conducting regions, ie, the SA and AV nodes. We suggest that the low single channel conductance of mCx30.2 contributes to the slow propagation velocities within nodal regions.

In general, the expression pattern of mCx30.2 resembles that of Cx45 as demonstrated using $Cx45^{+/LacZ}$ mice with targeted replacement of the Cx45-coding region with the lacZ reporter gene.[19] By combining β-gal labeling for lacZ and immunofluorescence for mCx30.2, we found coexpression of Cx45 and mCx30.2 in SA node, AV node, and A-V bundle (Figure III-B and Figure I-S in online supplement).

In contrast to earlier reports,[16] we did not detect mCx30.2 protein expression in vascular smooth muscle cells of several tissues that we analyzed by immunofluorescence (data not shown). It is possible that the low mCx30.2 expression levels in the cell types examined are below the detection limit of our mCx30.2 antibodies. Earlier reports of expression might have been because of cross reactivity of the mCx30.2 antibodies used.[16] Nevertheless, our RT-PCR analyses revealed transcripts of mCx30.2 in heart, brain, liver, lung, kidney, and testis. This expression pattern might be because of the expression of the mCx30.2 transcript in blood vessels of these tissues.

Functional Properties of Homo- and Hetero-typic Junctions

We demonstrated that mCx30.2 channels exhibit weak sensitivity to V_j and a very low single channel conductance, ≈9 pS. When expressed in *Xenopus* oocytes or HeLa cells, little

if any reduction in G_j was evident until V_js exceeded ±80 mV. Attachment of EGFP to the carboxy terminus of mCx30.2 did not appear to have any measurable effects on single channel conductance or gating properties. Channels formed of human Cx31.9, the human orthologue of mCx30.2, were reported to exhibit similar properties, although the single channel conductance was somewhat larger, ie, 12 to 15 pS.[17] Cx36, the major neuronal connexin, also forms channels with weak sensitivity to V_j and a low single channel conductance (≈15 pS),[22,23] but exhibits only 30% to 40% sequence identity to mCx30.2 or Cx31.9.[17] The low unitary conductance of mCx30.2 is reflected in the low unitary conductances of the heterotypic channels formed by pairing mCx30.2 with other cardiac connexins, ie, Cx40 (18 pS), Cx43 (18 pS), or Cx45 (17 pS). These conductances are close to the values of 17, 17, and 14 pS, respectively, predicted by the series arrangement of these heterotypic combinations according to $\gamma_{AB}=2 \cdot \gamma_A \cdot \gamma_B/(\gamma_A+\gamma_B)$, where γ_A and γ_B represent the conductances of homotypic GJ channels of connexins A and B. Values of γ for Cx40, Cx43 and Cx45 are ≈180, 115, and 32 pS, respectively, as previously described.[24,25,20]

Our dye transfer studies showed that mCx30.2 GJs are permeable to positively and negatively charged dyes such as Neurobiotin, EtBr, DAPI, Alexa Fluor-350. However, we did not detect transfer of Lucifer yellow or propidium iodide, suggesting that mCx30.2 channels, while not particularly selective on the basis of charge, are size-restrictive with a cut-off to tracers >400 Da molecular mass. Furthermore, this restricted permeability appears to be reflected in the efficacy of Neurobiotin transfer, which is low compared with that of Cx43-expressing cells (Figure 5D). Previous reports indicated that HEK cells expressing Cx31.9 lacked transfer of Lucifer yellow or ethidium bromide.[15] Whether permeability of mCx30.2 channels to EtBr observed in this study represents a difference between Cx31.9 and mCx30.2 or is because of different detection sensitivity remains to be determined.

We have demonstrated expression of mCx30.2 in the SA node, AV node, and A-V bundle. It was previously reported that cells in the SA node express Cx45, cells in the AV node as well as in the A-V bundle express Cx40 and Cx45[7,6] and Purkinje cells express Cx40 and Cx43. Within the atrial and ventricular myocardium, atrial cardiomyocytes predominantly express Cx40 and Cx43, whereas Cx43 is the major connexin in working ventricular myocytes.[4] These patterns of expression suggest that mCx30.2 might interact with Cx40 or Cx45 within the SA and AV nodal regions and with Cx43 in adjacent regions that interconnect the atrial myocardium and the ventricular conduction system.

We have examined whether mCx30.2 was capable of interacting with the other cardiac connexins in heterotypic combinations after expression in HeLa cells. We found that all 3 possible heterotypic junctions with mCx30.2, mCx30.2/Cx40, mCx30.2/Cx45, and mCx30.2/Cx43, were functional under these conditions. In each case, the steady-state G_j-V_j relations were asymmetric, but differed in the degree and direction of asymmetry. An important point in understanding the G_j-V_j relations of these junctions is the small unitary conductance of the mCx30.2 hemichannel. When paired with a hemichannel that exhibits a larger unitary conductance, a larger fraction of V_j will drop across the mCx30.2 hemichannel because of its low conductance (inferred to be ≈18 pS, ie, 2-fold higher than that of the gap junction channel). This increases the fraction of V_j that drops across the mCx30.2 hemichannel and thus decreases the probability that gating events will occur in Cx40, Cx43, or Cx45 hemichannels paired with mCx30.2. This effect would be smallest in Cx45/mCx30.2 heterotypic junctions because of the relatively low conductance of Cx45 hemichannels (≈64 pS). Similar effects of unitary conductance of component hemichannels on V_j-gating has been described for Cx43/Cx45 channels.[20] Based on the G_j-V_j dependent properties of the heterotypic junctions examined here and knowing that both Cx43 and Cx45

have a negative gating polarity,[25,20] whereas Cx40 exhibits a positive one,[26] we ascribe a negative gating polarity to mCx30.2.

Our data show that mCx30.2/Cx40 junctions in HeLa transfectants exhibit significant rectification (Figure 6B and 6C). This property would facilitate the spread of excitation from the cells expressing Cx40 to neighboring cells expressing mCx30.2 and impede spread in the opposite direction. In the heart, normal signal propagation is oriented downstream along atrium, AV node, A-V bundle and branches, Purkinje terminals, and working myocytes of ventricles. Along this pathway, action potentials might encounter several types of heterotypic and heteromeric junctions containing mCx30.2. Transjunctional voltage at the edge of an excitation front could be relatively high in regions with slow velocities of propagation, such as the AV node. Such V_js across junctions with strong G_j-V_j dependence, eg, mCx30.2/Cx45 could modulate g_j, thereby impeding signal transfer in one direction and facilitating it in the opposite direction. Formation of heterotypic junctions containing mCx30.2 could contribute, at least in part, to electrical signal transfer from the AV node to ventricular working myocytes. However, to what extent heterotypic junctions form within the cardiac conduction system is not known. Furthermore, it is possible that mCx30.2 can form heteromeric channels with coexpressed Cx45. Future studies will have to show whether such heteromeric channels will also exhibit a low unitary conductance.

In summary, we have analyzed expression of the mCx30.2 gene and found that mCx30.2 is abundantly expressed in the nodal regions of the mouse heart. mCx30.2 can form heterotypic channels with all major cardiac connexins in transfected HeLa cells and is likely to influence and regulate the propagation of electrical signals in the heart.

Supplementary Material

Refer to Web version on PubMed Central for supplementary material.

Acknowledgments

This study was supported by grants of the German Research Association (Wi 270/25–1,2) to K.W. and by NIH Grants, GM54179 to V.K.V. and NS036706 to F.F.B.

References

1. Söhl G, Willecke K. Gap junctions and the connexin protein family. Cardiovasc Res. 2004; 62:228–232. [PubMed: 15094343]
2. Bukauskas FF, Verselis VK. Gap junction channel gating. Biochim Biophys Acta. 2004; 1662:42–60. [PubMed: 15033578]
3. Gros DB, Jongsma HJ. Connexins in mammalian heart function. Bioessays. 1996; 18:719–730. [PubMed: 8831288]
4. Severs NJ, Dupont E, Coppen SR, Halliday D, Inett E, Baylis D, Rothery S. Remodelling of gap junctions and connexin expression in heart disease. Biochim Biophys Acta. 2004; 1662:138–148. [PubMed: 15033584]
5. Lo CW. Role of gap junctions in cardiac conduction and development: insights from the connexin knockout mice. Circ Res. 2000; 87:346–348. comment] [editorial. [PubMed: 10969030]
6. van Rijen HV, van Veen TA, van Kempen MJ, Wilms-Schopman FJ, Potse M, Krüger O, Willecke K, Opthof T, Jongsma HJ, de Bakker JM. Impaired conduction in the bundle branches of mouse hearts lacking the gap junction protein connexin40. Circulation. 2001; 103:1591–1598. [PubMed: 11257090]
7. Coppen SR, Dupont E, Rothery S, Severs NJ. Connexin45 expression is preferentially associated with the ventricular conduction system in mouse and rat heart. Circ Res. 1998; 82:232–243. [PubMed: 9468194]

8. Verheijck EE, van Kempen MJ, Veereschild M, Lurvink J, Jongsma HJ, Bouman LN. Electrophysiological features of the mouse sinoatrial node in relation to connexin distribution. Cardiovasc Res. 2001; 52:40–50. [PubMed: 11557232]
9. Reaume AG, De Sousa PA, Kulkarni S, Langille BL, Zhu D, Davies TC, Juneja SC, Kidder GM, Rossant J. Cardiac malformation in neonatal mice lacking connexin43. Science. 1995; 267:1831–1834. [PubMed: 7892609]
10. Kirchhoff S, Kim JS, Hagendorff A, Thönnissen E, Krüger O, Lamers WH, Willecke K. Abnormal cardiac conduction and morphogenesis in connexin40 and connexin43 double-deficient mice. Circ Res. 2000; 87:399–405. see comments. [PubMed: 10969038]
11. Simon AM, McWhorter AR, Dones JA, Jackson CL, Chen H. Heart and head defects in mice lacking pairs of connexins. Dev Biol. 2004; 265:369–383. [PubMed: 14732399]
12. Plum A, Hallas G, Magin T, Dombrowski F, Hagendorff A, Schumacher B, Wolpert C, Kim J, Lamers WH, Evert M, Meda P, Traub O, Willecke K. Unique and shared functions of different connexins in mice. Curr Biol. 2000; 10:1083–1091. [PubMed: 10996788]
13. Alcolea S, Jarry-Guichard T, de Bakker J, Gonzalez D, Lamers W, Coppen S, Barrio L, Jongsma H, Gros D, van Rijen H. Replacement of connexin40 by connexin45 in the mouse: impact on cardiac electrical conduction. Circ Res. 2004; 94:4–6. [PubMed: 14715530]
14. Taffet SM, Jalife J. Swapping connexin genes: how big is the gap? Circ Res. 2004; 94
15. Nielsen PA, Beahm DL, Giepmans BN, Baruch A, Hall JE, Kumar NM. Molecular cloning, functional expression, and tissue distribution of a novel human gap junction-forming protein, connexin-31.9. Interaction with zona occludens protein-1. J Biol Chem. 2002; 277:38272–38283. [PubMed: 12154091]
16. Nielsen PA, Kumar NM. Differences in expression patterns between mouse connexin-30.2 (Cx30.2) and its putative human orthologue, connexin-31.9. FEBS Lett. 2003; 540:151–156. [PubMed: 12681499]
17. White TW, Srinivas M, Ripps H, Trovato-Salinaro A, Condorelli DF, Bruzzone R. Virtual cloning, functional expression, and gating analysis of human connexin31.9. Am J Physiol Cell Physiol. 2002; 283:C960–C970. [PubMed: 12176752]
18. Shapiro MB, Senapathy P. RNA splice junctions of different classes of eukaryotes: sequence statistics and functional implications in gene expression. Nucleic Acids Res. 1987; 15:7155–7174. [PubMed: 3658675]
19. Krüger O, Plum A, Kim JS, Winterhager E, Maxeiner S, Hallas G, Kirchhoff S, Traub O, Lamers WH, Willecke K. Defective vascular development in connexin 45-deficient mice. Development. 2000; 127:4179–4193. [PubMed: 10976050]
20. Bukauskas FF, Bukauskiene A, Verselis VK, Bennett MVL. Coupling asymmetry of heterotypic connexin 45/connexin 43-EGFP gap junctions: Properties of fast and slow gating mechanisms. Proc Natl Acad Sci U S A. 2002; 99:7113–7118. [PubMed: 12011467]
21. Willecke K, Eiberger J, Degen J, Eckardt D, Romualdi A, Güldenagel M, Deutsch U, Söhl G. Structural and functional diversity of connexin genes in the mouse and human genome. Biol Chem. 2002; 383:725–737. [PubMed: 12108537]
22. Srinivas M, Rozental R, Kojima T, Dermietzel R, Mehler M, Condorelli DF, Kessler JA, Spray DC. Functional properties of channels formed by the neuronal gap junction protein connexin36. J Neurosci. 1999; 19:9848–9855. [PubMed: 10559394]
23. Teubner B, Degen J, Sohl G, Guldenagel M, Bukauskas FF, Trexler EB, Verselis VK, De Zeeuw CI, Lee CG, Kozak CA, Petrasch-Parwez E, Dermietzel R, Willecke K. Functional expression of the murine connexin 36 gene coding for a neuron-specific gap junctional protein. J Membr Biol. 2000; 176:249–262. [PubMed: 10931976]
24. Bukauskas FF, Elfgang C, Willecke K, Weingart R. Biophysical properties of gap junction channels formed by mouse connexin40 in induced pairs of transfected human HeLa cells. Biophys J. 1995; 68:2289–2298. [PubMed: 7544165]
25. Bukauskas FF, Bukauskiene A, Bennett MV, Verselis VK. Gating properties of gap junction channels assembled from connexin43 and connexin43 fused with green fluorescent protein. Biophysical Journal. 2001; 81:137–152. [PubMed: 11423402]

26. Valiunas V, Weingart R, Brink PR. Formation of heterotypic gap junction channels by connexins 40 and 43. Circ Res. 2000; 86:E42–E49. [PubMed: 10666425]

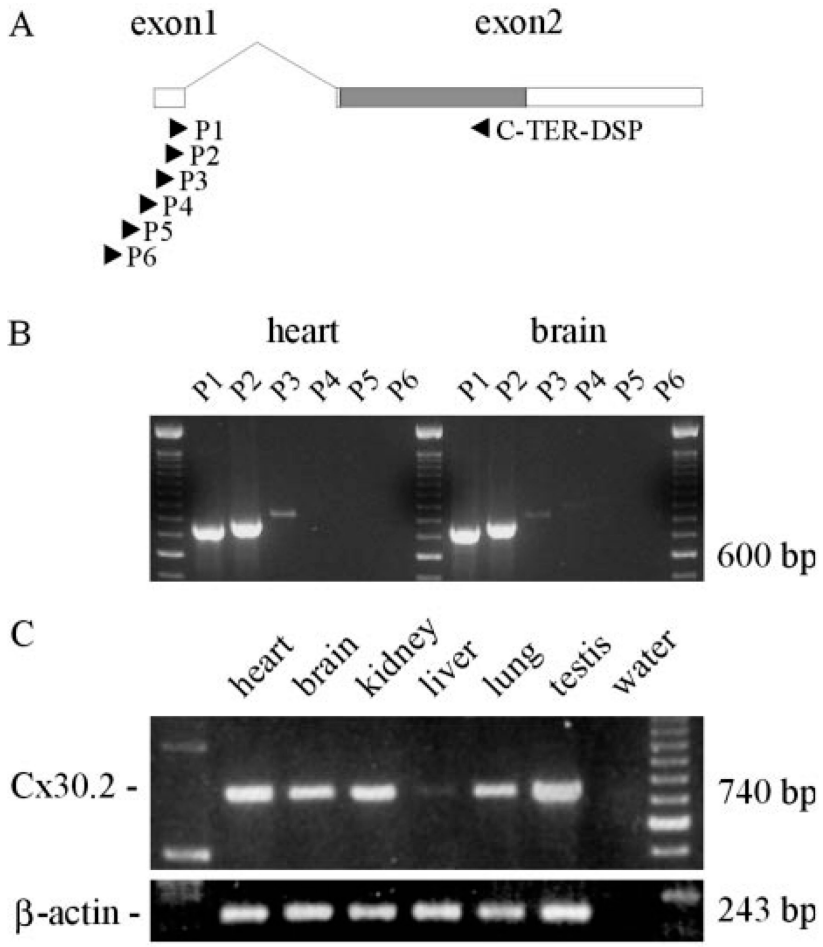

Figure 1.

RT-PCR analysis of adult mouse tissues. A, The mCx30.2 gene includes an untranslated exon1 and an exon2 containing the whole coding region (dark shaded) and the 3′-untranslated region. The primers (P1-P6) indicated by arrowheads were used for the PCR reaction (for details see Methods in online data supplements). B, Determination of the transcriptional start site was performed with P1-P6 primers and cDNA from heart and brain. C, Intron-spanning RT-PCR of different mouse tissues revealed the expression of the same mCx30.2 transcript isoform in heart, brain, kidney, lung, testis, and very weakly in liver. cDNA of β-actin served as a control.

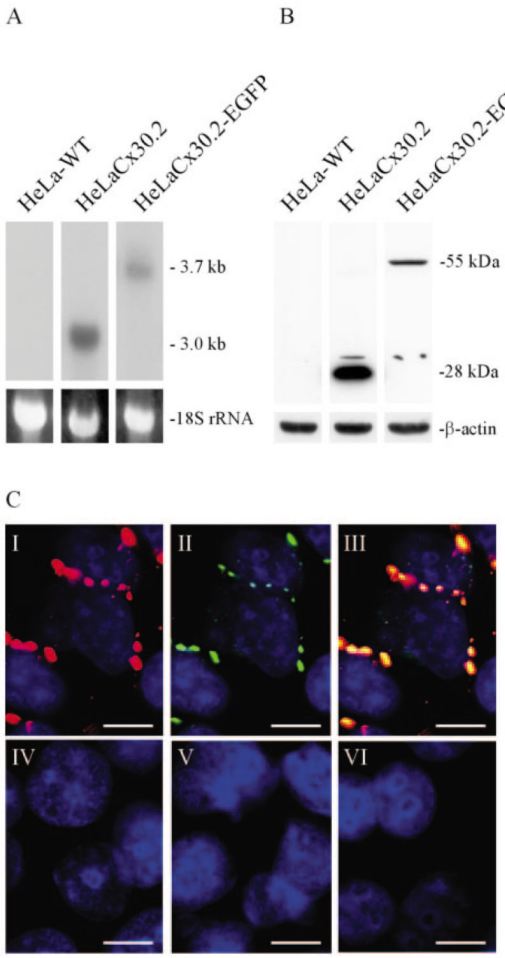

Figure 2.

mCx30.2 and mCx30.2-EGFP expression in HeLa transfectants. A, Northern blot analysis of HeLa wild-type, HeLaCx30.2 and HeLaCx30.2-EGFP cells. Ethidium bromide staining of 18S rRNA demonstrates equal loading of total RNA. Blotted RNA was hybridized to a ^{32}P-labeled mCx30.2 probe of the coding region corresponding to the N-terminal portion (nt +1 to nt +530). B, Immunoblot analysis of HeLa-WT, HeLaCx30.2-EGFP and HeLaCx30.2 cells using affinity purified antibodies raised to peptides of the cytoplasmic loop and C-terminal region of mCx30.2. Analysis of β-actin indicates that equal amounts of protein were loaded. C, Immunofluorescence analysis of HeLa cells expressing mCx30.2-EGFP (I-III), Cx40 (IV), Cx43 (V), and Cx45 (VI) with affinity purified antibodies to mCx30.2. Punctate staining of junctional plaques revealed by immunofluorescence (I) and EGFP signals (II) colocalize (III). Cx40, Cx43, and Cx45 do not react with mCx30.2 antibodies (IV-VI). The nuclei of the cells were stained with Hoechst 33528 (blue). Scale bars, 10 μm.

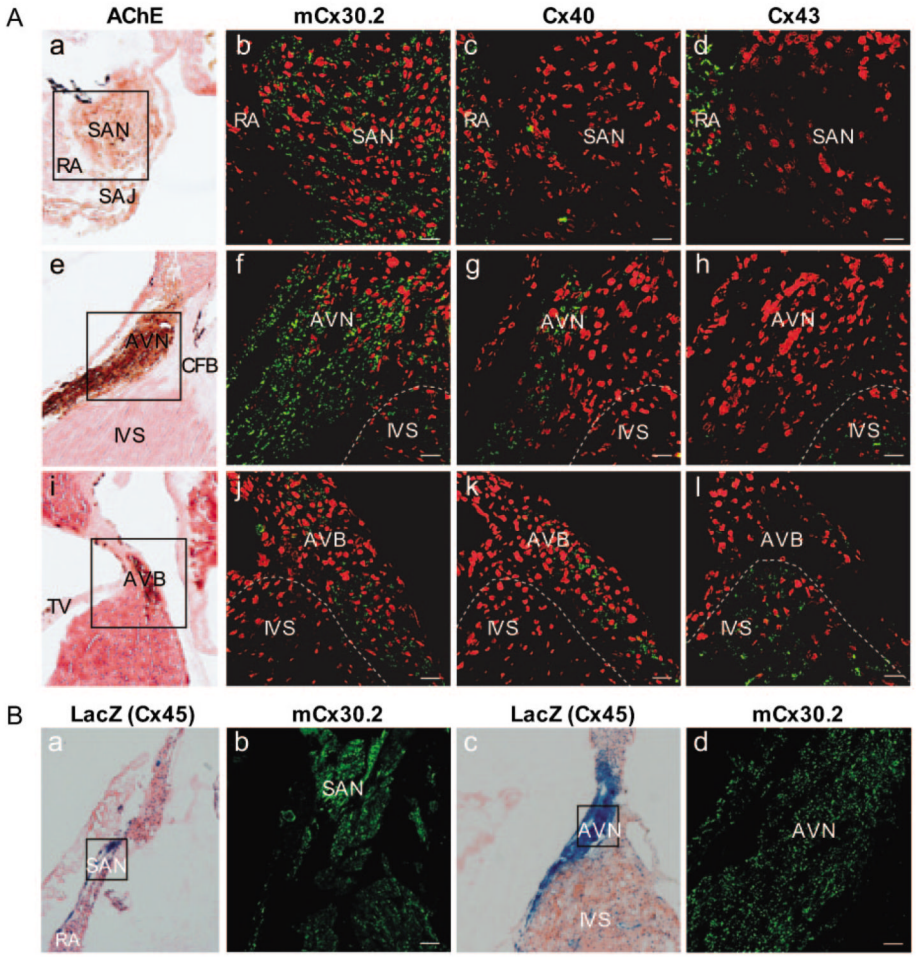

Figure 3.

Immunofluorescence analysis of mCx30.2 expression pattern and colocalization with other cardiac connexins. A, Shown are immunofluorescence images (green) of mCx30.2 (b,f,j), Cx40 (c,g,k) and Cx43 (d,h,l) in serial sections from adult mouse heart. Left column shows bright field images (a,e,i) stained for acetylcholine esterase (AChE); squares indicate approximate regions from which immunofluorescence images were acquired. Images in rows (a-d), (e-h) and (i-l) correspond to the regions of the SA node, AV node, and A-V bundle, respectively. Immunostaining of mCx30.2 is visible in the SA node (b), AV node (f), and A-V bundle (j). Cx40 immunostain-ing in the AV node and A-V bundle rarely overlaps with that of mCx30.2, but not within the SA node. Cx43 is not expressed in the SA node, AV node and A-V bundle, but in the atrial and ventricular working myocytes (d,h,l). Dashed lines separate AV-nodal region and A-V bundle from working myocardium. Used abbreviations: AVB, A-V bundle; AVN, AV node; CFB, central fibrous body; IVS, interventricular septum; RA, right atrium; SAN, SA node; SAJ, sinoatrial junction; TV-tricuspid valve. Nuclei of the cells were stained in red with propidium iodide. Scale bars, 20 μm. (B) Coexpression of Cx45 and mCx30.2 in SA node (a,b) and AV node (c,d) of Cx45LacZ mouse. Immunofluorescence signals (b,d; in green) abundantly overlap with LacZ signals (a,c; in blue) in both nodal regions. Scale bars, 20 μm.

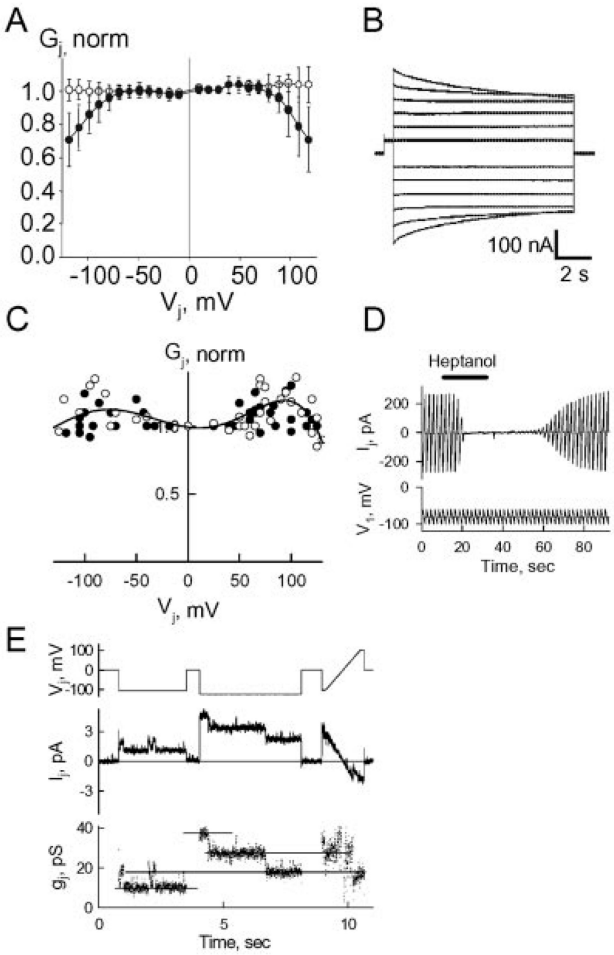

Figure 4.

Voltage and chemical gating of mCx30.2 and mCx30.2-EGFP. A, Voltage dependence of mCx30.2 in *Xenopus* oocytes. Graph of normalized initial and steady-state G_js (open and filled symbols, respectively) as a function of V_j. Each point represents mean G_j obtained from 11 oocyte pairs. B, Representative junctional currents for V_j steps up to ±120 mV in 20 mV increments. A +20 mV V_j step, 200 ms in duration, preceded each long-duration (30 s) V_j step. C, G_j-V_j plot determined in HeLaCx30.2 (open circles) and HeLaCx30.2-EGFP (filled circles) cell pairs. Solid line is a fit of the data to a regression function of the 5th order. D, Application of heptanol (2 mmol/L) produced full uncoupling of mCx30.2 homotypic junctions within ≈5 s. Recovery was fast and complete. E, V_j and I_j recordings and the resulting g_j demonstrating unitary gating events during voltage steps of −105 mV and −125 mV as well as a ramp of -/+100 mV. Single channels were visualized during the recovery from full uncoupling with CO_2. Single channel conductance in these recordings was found to be ≈9 pS (see horizontal lines).

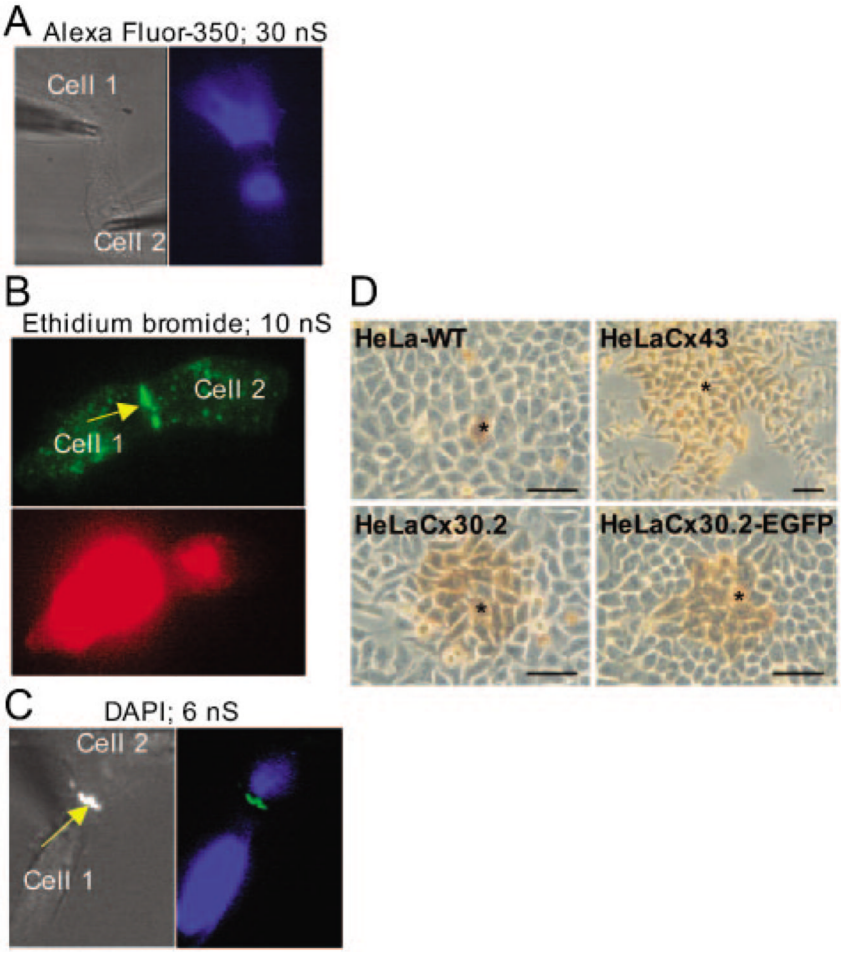

Figure 5.

Permeability of mCx30.2, mCx30.2-EGFP, and Cx43 junctions to dyes. A, Phase contrast and fluorescence images demonstrating Alexa Fluor-350 transfer in a HeLaCx30.2-EGFP cell pair; g_j=30 nS. Cell 1 was loaded with dye through a patch pipette (left-top). B, Fluorescence images of mCx30.2-EGFP (top; the arrow points to a junctional plaque) and EtBr (bottom) demonstrating EtBr transfer from cell 1 to cell 2; g_j=10 nS. C, Phase contrast image overlapping with fluorescence of mCx30.2-EGFP (left; the arrow points to a junctional plaque) and fluorescence image of DAPI (right); g_j=6 nS. D, Intercellular transfer of Neurobiotin measured 30 minutes after microinjection into HeLa-WT, HeLa-Cx43, HeLaCx30.2, and HeLaCx30.2-EGFP cells. Neurobiotin does not spread from the injected cell (asterisk) to neighboring cells in a monolayer of HeLa-WT cells, but readily spreads to first and second order neighbors in monolayers of HeLaCx30.2 and HeLaCx30.2-EGFP cells and even more extensively in a monolayer of HeLaCx43 cells. Scale bars, 50 μm.

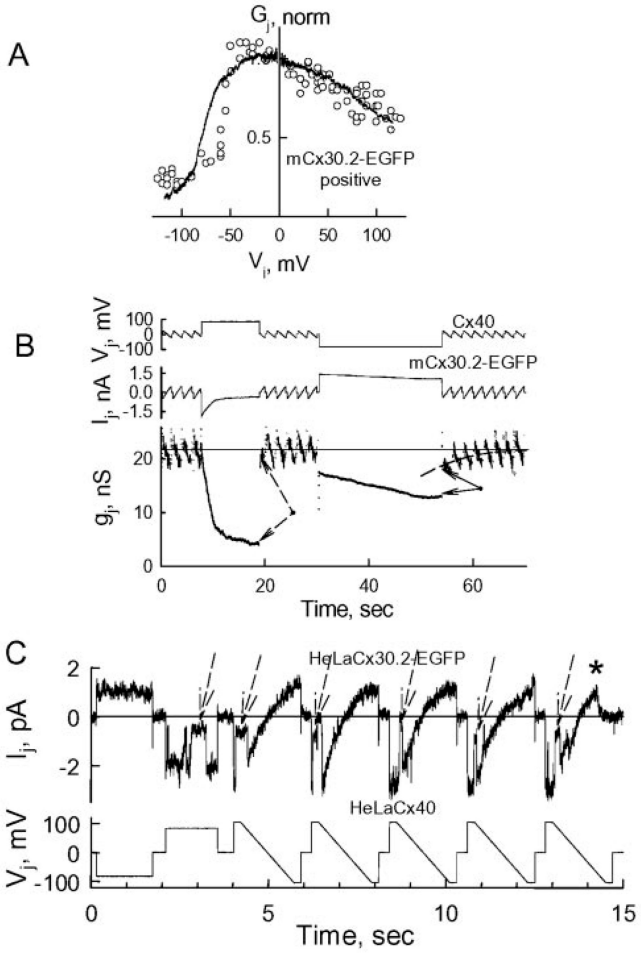

Figure 6.

Electrophysiological characterization of heterotypic mCx30.2-EGFP/Cx40 channels examined in cocultured HelaCx30.2-EGFP and HeLaCx40 cells. A, Normalized G_j–V_j plot shows highly asymmetric V_j gating. Data points (open circles) were measured at the ends of the voltage steps. Solid line was obtained applying V_j ramps of 120 s in duration. V_j is defined relative to the mCx30.2-EGFP side. B, Example of V_j, I_j and g traces obtained to voltage steps of 85 and −85 mV applied to the HeLaCx40 cell. Repeated voltage ramps of ±20 mV were used to assess g_j between the voltage steps. C, Representative I_j and V_j records measured during application of voltage steps and ramps to the HeLaCx40 cell. Gating transitions to the sub-state (dashed arrows) occurred more often when the mCx30.2 side was made relatively negative. The asterisk shows only one full closure of the channel that occurred at relative negativity of V_j on the Cx40 side.

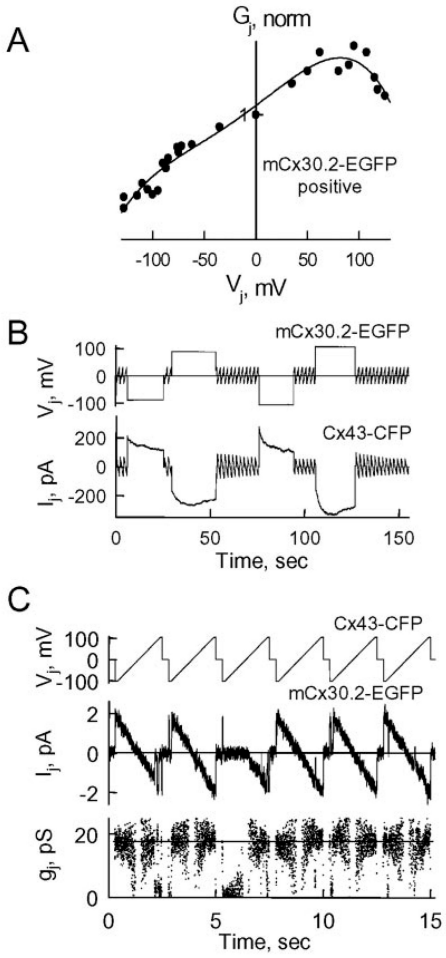

Figure 7.

Gating properties of heterotypic mCx30.2-EGFP/Cx43-CFP channels examined in cell pairs with junctional plaques formed between HeLaCx43-CFP and HeLaCx30.2-EGFP cells. A, Normalized G_j–V_j plot; V_j is defined relative to the mCx30.2-EGFP side. The solid line is a regression line of the fifth order fit to the data. B, Representative V_j and I_j records demonstrate asymmetric V_j gating in response to consecutive steps of −90, 90, −110, and 110 mV and repeated ramps of ±20 mV applied to the HeLaCx30.2-EGFP cell. Negative V_j steps induced a slow decrease in I_j whereas positive ones initially increased and then slowly decreased I_j. C, Single channel record obtained by applying voltage ramps (±105 mV) to the HeLaCx43-CFP cell shows a linear open channel I-V relationship and a single channel conductance of ≈18 pS.

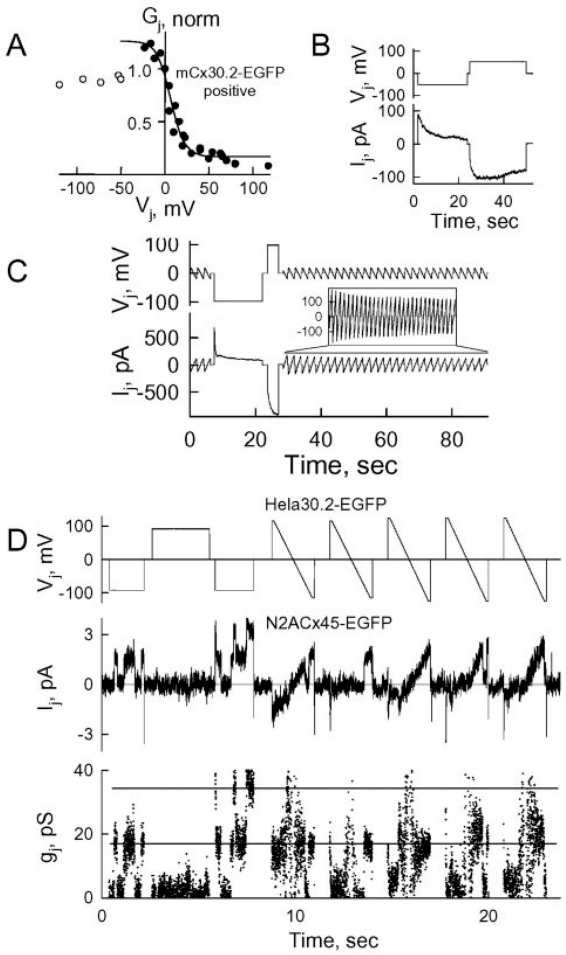

Figure 8.

Gating properties of heterotypic mCx30.2-EGFP/Cx45-EGFP channels examined in cocultured HeLaCx30.2-EGFP and N2ACx45-EGFP cells. A, Normalized G_j–V_j plot. The solid line is a fit of the data, shown in solid circles, to the Boltz-mann equation. B,C, Examples of V_j and I_j records demonstrate asymmetric V_j gating in response to voltage steps applied to the Cx45-EGFP side. Repeated voltage ramps of ±20 mV demonstrate reduction of I_j after a positive voltage step (see insert). D, I_j record of single channel in response to ±95 mV voltage steps and ramps (±100 mV) applied to the N2ACx45-EGFP cell. The single open channel I-V relation is essentially linear with a single channel conductance of ≈17 pS (horizontal lines in g_j-time plot).